Proceedings of ASME Turbo Expo 2016: Turbomachinery Technical Conference and Exposition
GT2016
June 13-17, 2016, Seoul, South Korea

GT2016-57896

OPTIMIZING SURGE MARGIN AND EFFICIENCY OF A TRANSONIC COMPRESSOR

Georgios Goinis, Eberhard Nicke
German Aerospace Center (DLR)
Institute of Propulsion Technology
Linder Höhe, 51147 Cologne, Germany
Email: georgios.goinis@dlr.de

ABSTRACT

It has been shown in several cases that casing treatments can improve the surge margin of a compressor. The question that is often left unanswered when designing and optimizing a casing treatment for a given compressor stage is whether the casing treatment can still improve the performance and surge margin when used on an aerodynamically improved rotor.

The current work includes the influence of the rotor geometry and casing geometry in the analysis. Several optimizations with equal objectives, to improve surge margin and efficiency, were performed. First the different components were optimized separately. The possible impact of optimizing the rotor, the casing geometry and the casing treatment on surge margin and efficiency are compared in terms of global performance and aerodynamic effects. It is then analyzed how combinations of optimized geometries perform. Of particular interest is how the circumferential grooves perform when used in combination with the optimized blade geometry.

The optimizations were performed using state of the art CFD and optimization procedures. Constraints on boundary conditions, mass flow rates and stresses were applied in order not to change the behavior of the compressor at design point significantly or to deteriorate the structural mechanics.

NOMENCLATURE

ADP Aerodynamic design point
CG Circumferential groove, also Casing groove
CT Casing treatment
HF High fidelity
LE Leading edge
LF Low fidelity
MVDR Meridional velocity density ratio
OP Operating point
RANS Reynolds-averaged Navier-Stokes
RPM Revolutions per minute
TE Leading edge

Introduction

Casing treatments (CTs) are applied to increase the surge margin of a compressor. As CTs influence the flow through the compressor at all operating points, the performance characteristics are also affected at working conditions, clearly away from the surge margin. This influence of CTs on the flow at design point conditions can be negative, especially regarding efficiency. Therefore it is of high importance to not only take into account the surge margin when designing CTs but also the efficiency.

The evaluation of a newly designed or optimized CT is usually done in comparison to the untreated smooth wall configuration. Inevitably the question arises how much of

the reported gain in surge margin and in some cases even efficiency is due to an inferior design of the reference smooth wall configuration. It is still unclear whether including a CT in the design of a new compressor stage can lead to higher overall surge margin and efficiency compared to a new, state of the art design without treatment.

One common type of CTs are axisymmetric circumferential grooves (CGs). So far the design of the grooves is mainly based on empirical results rather than established design criteria. Usually the shape, count and location of the grooves are changed for a limited number of configurations which are then compared to study the flow effects. Only recently specific geometric parameters are analysed extensively, mainly due to the advances in CFD technology. Many of these studies were done for subsonic compressors and only few are available for transonic compressors. But as the flow physics of subsonic and transonic compressors differ significantly the transferability of the results is limited. Furthermore, the results are sometimes contradictory regarding an optimal design of the groove, underlining the need for further research.

Circumferential grooves can be simulated using steady state CFD methods which is a big advantage regarding computational costs compared other types of CTs that need to be simulated using time accurate CFD. This is a main reason why they were chosen for the study at hand and for many studies in literature as well, despite the fact that the gain in surge margin is lower for circumferential grooves compared to other types of CTs such as axial slots or tip blowing CTs.

Recent studies of CGs for transonic compressors, comparing different groove geometries and configurations, have been done, amongst others, by Rabe & Hah (2002) [1], Perrot et al. (2007) [2] and Mueller et al. (2007) [3]. Rabe & Hah (2002) [1] conclude from their numerical and experimental studies that the traditional assumption that shallow grooves are inferior to deeper grooves does not hold for transonic compressors and better results can be obtained with shallow grooves. Furthermore they found that two shallow grooves near the leading edge are more effective than five grooves from leading to trailing edge and concluded that grooves placed near the leading edge are more efficient. They assume that the main mechanism leading to the increase in surge margin of the grooves is an alteration of the local flow distribution near the pressure side of the leading edge, which can be measured by how much the flow incidence at the pressure side of the leading edge is reduced. Perrot et al. (2007) [2] conducted a numerical investigation and found that only grooves close to the leading edge of the rotor are improving the results, as grooves more to the trailing edge of the rotor do not overlay the tip leakage vortex trajectory. They assume that CGs improve the surge margin by delaying the shift of the entropy frontier between the main flow and the secondary tip leakage flow to the inlet. The overall performance is increased by weakening the disturbing eddy zone. Mueller et al. (2007) [3] studied experimentally and numerically different shallow and deep groove configurations and found the deep grooves to be more effective in increasing the operating range. Furthermore they found a higher coverage of the projected axial chord to be favourable in delaying stall inception towards lower mass flow rates. The deep grooves they examined could maintain the efficiency levels compared to the smooth wall configuration and the shallow grooves could even increase efficiency significantly. The grooves were found to reduce the blockage area inside the passage at small mass flow rates. They also found that the tip leakage flow gets deflected towards the axial direction much earlier. Experimental and numerical parametric studies, varying the axial location of a single casing groove on two subsonic compressors have been done by Houghton & Day (2011 & 2012) [4] [5]. Two good groove locations for improving the surge margin are identified. One close to the leading edge and the second at about 50% chord. Shallow grooves offer higher efficiency with only slightly lower surge margin improvement. Numerical and experimental studies with different groove numbers and sizes have been conducted by Wu et al. (2010) [6]. They analyzed the impact of different groove parameters, such as width and height, on the surge margin extension capabilities of the grooves and studied the flow effects. Automated optimization procedures are now very popular in the aerodynamic design of compressors. First optimization studies related to CGs have been conducted by Choi et al. (2010) [7] and Carnie et al. (2011) [8]. Choi et al. (2010) [7] showed an optimization of circumferential grooves for NASA Rotor 37, with two free parameters, groove width and depth. Carnie et al. (2011) [8] optimized casing grooves, also for NASA Rotor 37. They allowed six grooves to change in height independently. The width of the grooves could change but was the same for all grooves. Both studies report a stall margin improvement with nearly no loss in peak

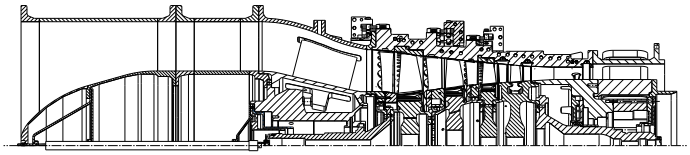

FIGURE 1. **Rig250 flow path**

RPM	12960 [1/min]
Mass flow rate (reduced)	46.3 [kg/s]
Total pressure ratio	4.82 [-]
Ma_{rel} (rotor 1 inlet, ADP)	1.21 [-]

TABLE 1. **Specifications of Rig250 at ADP conditions (100% speed)**

efficiency. This leads back to the initial question of how much of the improvement has to be attributed to the design of Rotor 37, which can be described as slightly outdated and thus suboptimal from today's point of view, and how much is due to sophisticated CT features.

In this study an optimization not only for the CT is conducted but for the annulus and rotor blade shape as well. The results are compared and it is analyzed how each part can contribute to an improved design. Of particular interest is how an optimal solution for the entire design space can be found. This includes the question how a CT design that has been optimized for the reference geometry will perform in conjunction with an optimized rotor.

TEST CASE

The test case used for this study is the first stage of DLR's research compressor Rig250 (see figure 1) [9], a 4.5 stage transonic axial compressor. The computational domain includes the IGV as well as the first rotor and stator. The main design parameters of Rig250 are listed in table 1.

To effectively increase the surge margin by applying CTs, it is a prerequisite that the rotor is tip critical [10]. The onset of (numerical) surge of the test configuration has been analyzed to be certain the configuration used in this study is tip critical. At 90% speed the first stator is closed by 8° for $n/N \leq 90\%$ in agreement with the guide vane schedule. This has been done to make sure that even with a high surge margin increase of the rotor, the rotor is still limiting the stability of the stage and not the stator.

OPTIMIZATION STRATEGY

Setting up the optimization procedure is a crucial aspect of any optimization especially if the available computational power is a limiting factor and has to be used in the best possible way.

In order to achieve the objectives of an optimization appropriate fitness functions and boundary conditions have to be defined. A procedure to perform all necessary simulations that enable calculating the fitness functions and constraints has to be set up, usually referred to as the process chain of the optimization. Given that the computational resources are a limiting factor, which is the case for almost all complex 3D-CFD optimizations, the computational costs of running the process chain once will define the maximum number of process chain runs and hence the total number of geometries that can be evaluated during the optimization.

This leads to a trade-off between the convergence of the optimization and the fidelity of the simulations. If the fidelity of the process chain is unnecessarily high, too few geometries will be simulated, limiting the optimization progress. If on the other hand the fidelity of the process chain is too low, the fitness function values will not be obtained with the accuracy needed to achieve consistent results.

The optimization studies presented herein aim at improving the surge margin of a transonic compressor. It is therefore important to determine the surge margin for every new geometry during the optimization with a high accuracy, yielding in a complex and costly procedure which has to be implemented in the process chain. However, the low uncertainty in predicting the numerical surge limit is seen as a necessity to obtain the desired information of relations between geometric and performance parameters, justifying the additional computational effort needed. On the other hand, as stated before, a sufficient number of geometries that can be simulated with the computational resources available has to be guaranteed for a successful optimization.

In this context, it is important to notice that the demands on the setup are different for optimizations compared to non-optimization cases. For an optimization it is sufficient to obtain qualitatively correct results. It is not necessary to get the absolute values right. Regarding the surge margin, the study at hand is based on the assumption that geometries reaching a higher numerical surge margin during the optimization will also reach a higher surge mar-

gin in reality; but the absolute values might be different.

There are several factors that influence the computational cost and fidelity of one process chain run. The most important ones are the following:

1. The number of operating points
2. The size and quality of the computational mesh
3. The convergence settings
4. The accuracy of determining the surge margin

Factors influencing the convergence of the optimization are the number of objectives, the number of free parameters and the complexity of the problem including the constraints that have to be met.

There are certain possibilities in significantly speeding up the convergence of the optimization which have been applied in this study:

1. Usage of two process chains of different fidelity
2. Extensive usage of surrogate models (Co-Kriging)

The strategy which has been followed herein to tackle the problem of limited computational power is to set up two process chains. One with a high accuracy in determining the surge margin and a second with a lower accuracy and less operating points. A multi fidelity optimization strategy using Co-Kriging methods is used based on these two process chains of different fidelity.

Parameterization

The blades are defined by a radial stacking of seven airfoils. A sketch of the airfoil parameterization is given in figure 2. Parameters which were selected as free parameters are stagger angle β_S, leading edge angle β_{LE}, trailing edge angle β_{LE}, suction side B-spline parameters and parameters for the thickness distribution as well as parameters for the leading edge shape. Six airfoils at relative radial heights of 10%, 25%, 50%, 75%, 90% and 100% were optimized. The airfoil at hub was left unchanged. In addition parameters for a circumferential shift of the profiles and for defining the axial position of the blade leading edge and trailing edge were used, influencing the chord length. In overall 70 parameters for the rotor were modified during the optimization.

The casing contour was parameterized using five spline construction points $P_1, \ldots, P_5$ as shown in fig. 3. The points were allowed to shift up- and downwards in radial direction by $\pm 2mm$, which is slightly more than the tip gap size. The

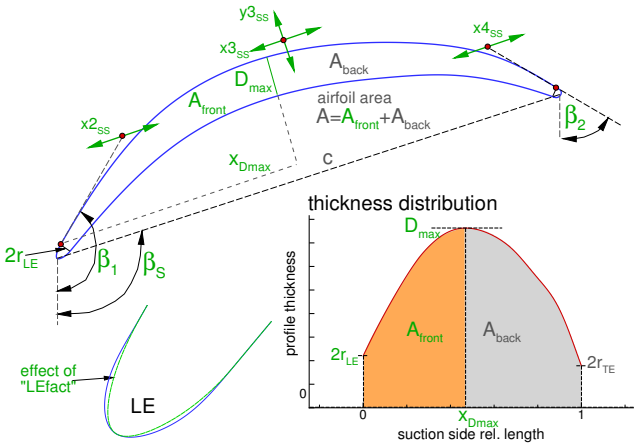

FIGURE 2. **Airfoil parameterization**

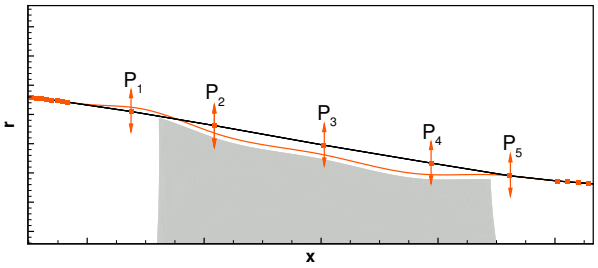

FIGURE 3. **Casing contouring parameterization**

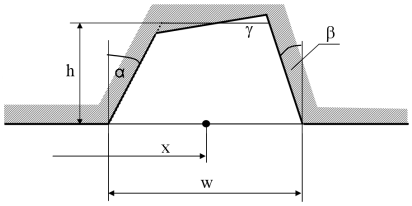

FIGURE 4. **Circumferential groove parameterization**

rotor geometry is adapted to the new casing such that the tip gap is kept constant all times.

The grooves are defined by six parameters, as shown in figure 4. The value ranges used for the optimization are listed in table 2. Groove width, height and axial position are normalized using the axial chord length at rotor tip c_{ax}.

During the optimizations it was continually checked not to introduce any limitations due to a too restrictive parameter range.

Parameter	Symbol	Min	Max
Groove position	x	$-0.3 \cdot c_{ax}$	$1.3 \cdot c_{ax}$
Groove width	w	$0 \cdot c_{ax}$	$0.3 \cdot c_{ax}$
Groove height	h	$0 \cdot c_{ax}$	$0.3 \cdot c_{ax}$
Upstream angle	α	$-75°$	$75°$
Downstream angle	β	$-75°$	$75°$
Angle of lid	γ	$-0.2rad$	$+0.2rad$

TABLE 2. Circumferential groove parameters; lengths based on axial chord of tip profile c_{ax}. Positions 0/1 correspond to tip LE/TE.

CFD Method

The CFD solver used in conjunction with the optimization tool is the Navier-Stokes solver *TRACE*, which is being developed specifically for turbomachinery flows at the DLR Institute of Propulsion Technology. Details on *TRACE* can be found in Ashcroft [11] and Becker [12]. A comparison of numerical results of CT flows obtained using *TRACE* and experimental data, showing good agreement, can be found in Voges et al. (2011) [13] and Schoenweitz et al. (2013) [14]. All optimizations were conducted using a RANS solver with a second order accurate Fromm scheme and van Albada limiter, $k\omega$ turbulence modeling and flux conserving mixing planes between the blade rows.

The meshing was not done with the aim to obtain mesh independent results but rather to obtain a mesh that still gets the deltas right. The mesh used for the optimization consists of approximately 1 million cells. That means the mesh can introduce an error on the fitness function values. However the variation of the error throughout the different geometries of the database is small enough, allowing to evaluate the different geometries against each other. A wall function approach is used at all surfaces. The circumferential grooves were coupled to the main mesh using a zonal boundary interface. The results discussed herein have been checked with a low Reynolds mesh of 4 million nodes.

Surge Point Determination

Two strategies for assessing the surge margin have been implemented. For the high fidelity (HF) process chain the surge margin is determined using an iterative approach based on a bisection method, which adapts the back pressure of the compressor in several simulation rounds until a further increase of back pressure by $\Delta p_{min.step}$ = 25Pa would lead to a failure in convergence according to the defined convergence criteria. A failure in convergence in this case is due to a continually decreasing mass flow as soon as the numerical stability limit is exceeded. It has been checked that no numerical stability issues leading to an abrupt termination of the simulation occurred.

For the low fidelity (LF) process chain the assessment of the surge margin is done indirectly by evaluating the flow values at a specific operating point close to the stability limit. This is much more approximate but has the advantage of needing only one CFD simulation to predict the surge margin.

Process Chain, Fitness Functions and Constraints

The same set-up was used for all optimizations, allowing a direct comparison of the results.

In order to calculate the fitness functions as well as aerodynamic and structural constraints of every new geometry a number of simulations have to be performed. The low and high fidelity process chains consists of the following main steps:

1. Parameter based geometry generation
2. Meshing
3. Pre-processing
4. CFD-simulation of all defined operating points including surge point iteration/estimation (HF/LF)
5. Structural mechanics computations
6. Post-processing
7. Calculation of fitness functions and constraints

The operating points that are simulated during the high fidelity process chain are shown in figure 5. The first operating point OP1 is fixed at a total pressure using a controller during the simulation. It is used to check the choking mass flow. OP2 is the maximum efficiency point which is determined using a maximum efficiency controller implemented in the CFD code. OP3 is the first operating point at 90% design speed, representing a working line operating point. OP3 is fixed at a constant static exit pressure. OP4 is a throttled operating point near the surge limit simulated using a mass flow controller fixing it at 30,5kg/s. OP5 is determined using the iterative process described above and is used to determine the surge margin. The convergence criteria for the CFD simulations are based on efficiency, mass flow and density residuum.

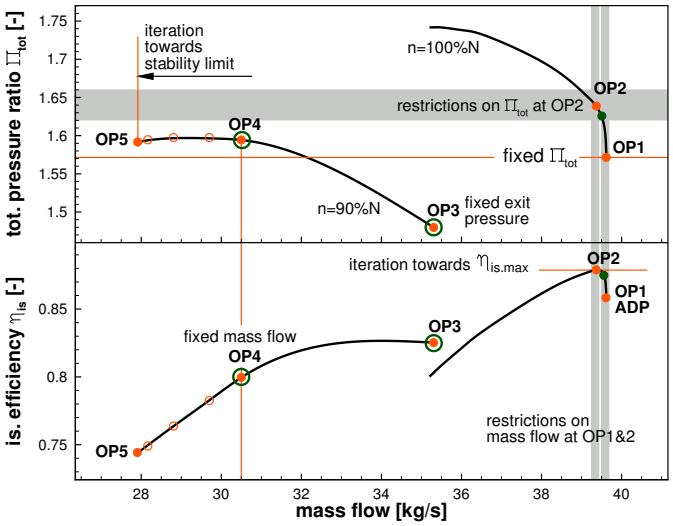

FIGURE 5. **Operating points of HF (orange) and LF (green) process, as well as constraints (grey)**

The low fidelity process chain consists of just three operating points and no surge point iteration and can therefore be processed in a fraction of the time necessary for the high fidelity (HF) process chain. The LF process chain includes one operation point LFOP1 which lies between OP1 and OP2 (green dot in fig. 5) and a second and third operating point which are equal to OP3 and OP4.

In order to optimize the surge margin whilst also taking into account the efficiency at design point conditions two fitness function are defined, the first aiming at increasing the maximum efficiency, the second at increasing the surge margin. The fitness functions are defined as follows:

1. Maximum efficiency of the component (IGV, rotor, stator) for the HF and LF process:

$$\eta_{is.max.HF} = \eta_{is.OP2}, \qquad \eta_{is.max.LF} = \eta_{is.LFOP1} \tag{1}$$

2. Surge margin criterion, as introduced by Reid and Moore (1978) [15], taking into account the mass flow and total pressure variation between the near stall operating point (HF=OP5, LF=OP4) and a reference point (OP3):

$$SM_{HF} = \frac{\Pi_{tot.OP5}}{\Pi_{tot.OP3}} \cdot \frac{\dot{m}_{OP3}}{\dot{m}_{OP5}} - 1 \tag{2}$$

$$SM_{LF} = \frac{\Pi_{tot.OP4}}{\Pi_{tot.OP3}} \cdot \frac{\dot{m}_{OP3}}{\dot{m}_{OP4}} - 1 \tag{3}$$

The relative increase in surge margin of a new design compared to the reference configuration reads:

$$\Delta SM = \frac{SM_{new}}{SM_{reference}} - 1 \tag{4}$$

Additionally constraints are set on the mass flow at OP1 and OP2 as well as the total pressure ratio at OP2 in order to keep the design point fixed within certain limits. As stated before, the CFD model was chosen in order to get the deltas right and not necessarily the absolute values. Therefore the absolute values imposed as constraints were chosen based on a simulation of the reference configuration with the CFD model used for the optimization. To make sure the structural mechanics are not deteriorated a constraint has been imposed on the maximum van Mises stresses of the rotor blade.

Optimization Tool

The optimization has been carried out using the DLR Institute of Propulsion Technology's optimization tool *AutoOpti*, which is a metamodel assisted multi-objective, multi-fidelity, multi-purpose optimization tool. Kriging and neural networks are used as surrogate models. Further information on *AutoOpti* can be found in Aulich and Siller (2011) [16] and Voß et al. (2014) [17].

RESULTS

Three separate optimizations, using the same fitness functions (eq. 1-3) were conducted: a) A single circumferential groove optimization, b) a casing contouring optimization and c) a rotor blade optimization. For the discussion of the results, only high fidelity results are considered. Figure 6 shows the Pareto fronts of these three optimizations along with the reference configuration. The highest gain in fitness function values can be achieved optimizing the rotor geometry with a maximum increase in peak efficiency of 0.5 percent points (pp) and surge margin of $\Delta SM = \frac{45\%}{36\%} - 1 = 25\%$. The optimization of the casing profile results in a maximum peak efficiency gain of 0.15% and maximum surge margin gain of 13%. It has to be noticed however that these values and the positions of the pareto fronts depend heavily on the restrictions imposed on OP1 and OP2 regarding mass flow and total pressure ratio. Tighter restrictions will reduce the increase in fitness

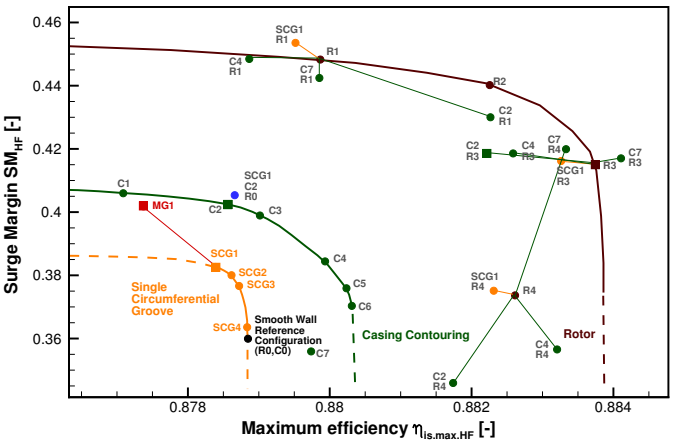

FIGURE 6. **Fitness function plot of Pareto optimal geometries and smooth wall reference configuration, C: casing contouring, R: rotor optimization, SCG: single circumferential groove optimization. (HF results only).**

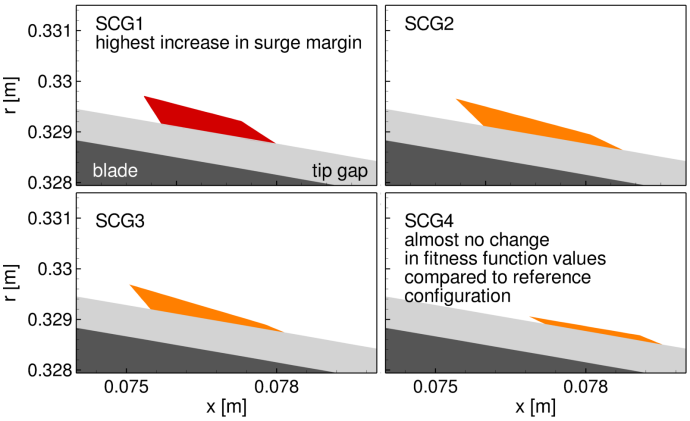

FIGURE 7. **Pareto optimal geometries of single groove optimization**

function values whereas unconstrained optimizations will lead to even higher fitness function values. Both optimizations can improve surge margin and efficiency at the same time. The optimization of a single circumferential groove could not improve the efficiency. A maximum gain in surge margin of 7% could be achieved.

Circumferential Groove Optimization

Fig. 7 shows the Pareto optimal grooves, highlighted in red is the groove which could achieve the highest surge margin increase (SCG1). All Pareto optimal grooves are located close to the leading edge at about 10% axial chord,

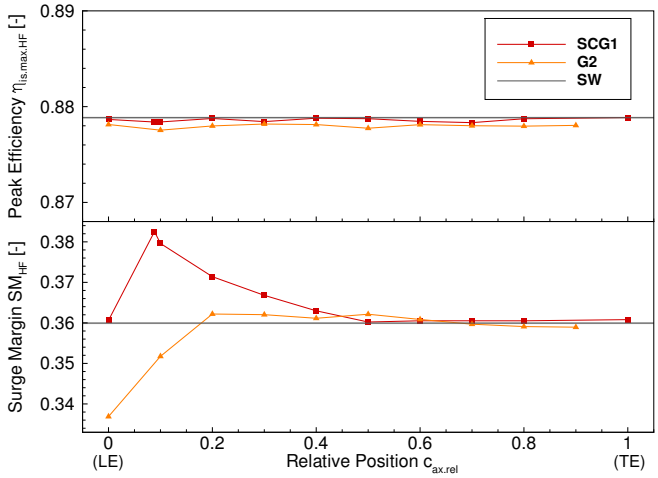

FIGURE 8. **Influence of single groove position on effectiveness**

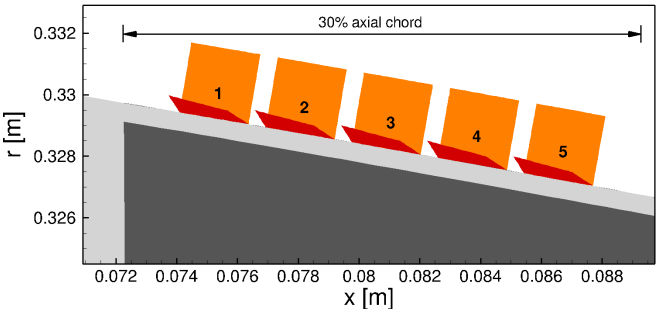

FIGURE 9. **Multiple groove configurations based on SCG1 (red) and G2 (orange)**

are relatively small in size and are inclined in an upwind direction.

The importance of the location can be further studied by changing the location of SCG1 from leading to trailing edge. Figure 8 shows how the effectiveness of SCG1 changes when the groove is shifted from leading edge to trailing edge. A positive effect can only be observed in the front part of the blade with an optimum at around 10% axial chord. The same study has been done with a groove of quadratic cross section of the same width as SCG1. With that groove (G2) no improvements in surge margin and a slightly higher loss in peak efficiency can be observed highlighting the importance of the cross sectional shape of the groove.

As the optimization of a single circumferential groove led to a small groove which is effective only in the front section of the blade it can be asked if more than one groove

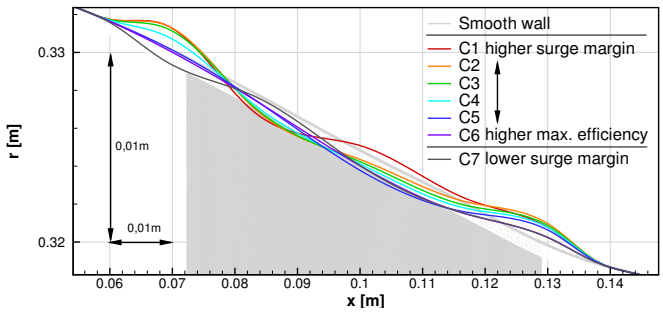

FIGURE 10. **Pareto optimal geometries (C1-C6) of casing contouring optimization. Note: Axes aspect ratio: (r/x)=(3/1)**

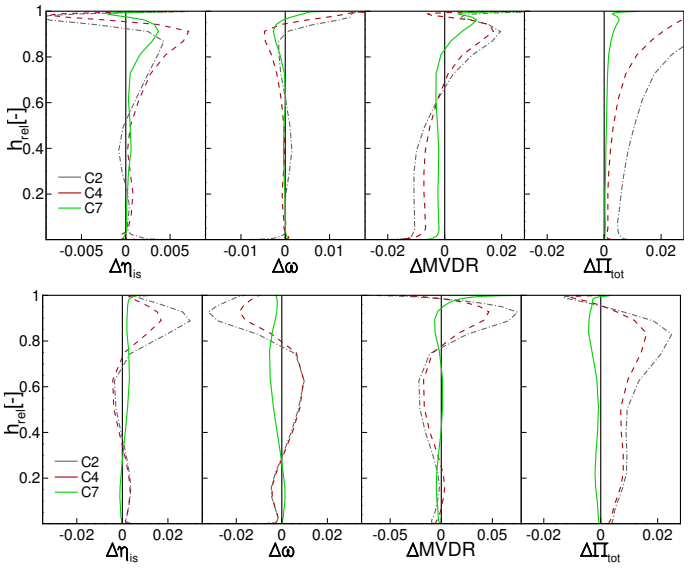

FIGURE 11. **Radial distributions (delta plots) at peak efficiency (OP2) (top) and near stall (OPA) (bottom) of selected annulus geometries in comparison to reference geometry C0**

can further improve the surge margin. An extensive study optimizing the number and geometry of multiple grooves is out of the scope of this study. However, a simple parametric study increasing the number of grooves from one to five in the front part of the blade has been carried out for SCG1 and G2 (see fig. 9). The best result regarding surge margin was obtained with four grooves of type SCG1 yielding in a surge margin increase of approximately 12% compared to the reference configuration. The fitness function values of this four groove configuration (MG1) are plotted in fig 6. Multiple grooves of type G2 could not improve the surge margin. With increasing groove number the loss in peak efficiency increases, as would be expected.

Casing Contouring Optimization

Figure 10 shows geometries of the casing contouring optimization. The corresponding fitness function values are highlighted in fig. 6. Geometries C1-C6 are Pareto optimal with descending surge margin and ascending peak efficiency.

It can be seen how the amplitude of the wave in the front section of the blade is increasing for higher surge margins. The amplitudes are even higher if no constraints are imposed on OP1 and OP2 leading to a further increase in surge margin improvement but at the cost of a decreasing choking mass flow. C7 has an amplitude in the opposite direction as compared to C1-C6 and a negative effect on the surge margin. Towards maximum peak efficiency (C1→C6) the casing becomes generally smoother with only a slight additional contraction in the rear part and a slight dent above the trailing edge left, compared to the reference casing C0.

At peak efficiency only a slight reduction in loss can be observed (fig. 11). The increase in peak efficiency of C4 is mainly due to a redistribution of the flow with an increase of MVDR at around 90% blade height and a reduction at blade sections below midspan. The loss coefficient in the vicinity of the casing, however, increases. Therefore the gain in peak efficiency obtained by C4 can be attributed to a sub optimal design of the rotor, not a reduction of loss mechanisms close to the casing. C2 shows the same tendency, but with an even higher loss near the casing, resulting in an overall peak efficiency which is equal to the reference design (C0). Near stall the loading at blade tip can be reduced by C1-C6 resulting in a weakened shock-vortex interaction due to a reduced shock intensity.

Casing C7 is not part of the Pareto front, as it is not improving the surge margin. The missing increase in MVDR and pressure ratio compared to C2 and C4 near surge at OPA suggests that C7 does not reduce the blade loading near surge. At peak efficiency however an overall reduction of loss can be observed pointing towards a different working principle as observed by Kröger et al. (2011) [18].

Rotor Optimization

The Pareto optimal rotor geometries all show a S-shape at the leading edge. The tip profiles are lower loaded compared to the reference design and all Pareto optimal rotors

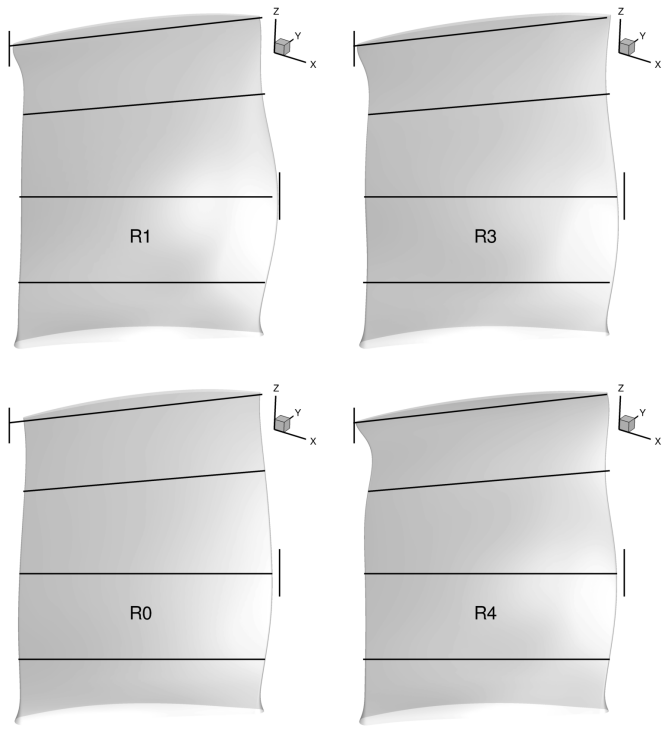

FIGURE 12. **Selected geometries of blade optimization in comparison with datum design (R0). Black lines all have same position and length**

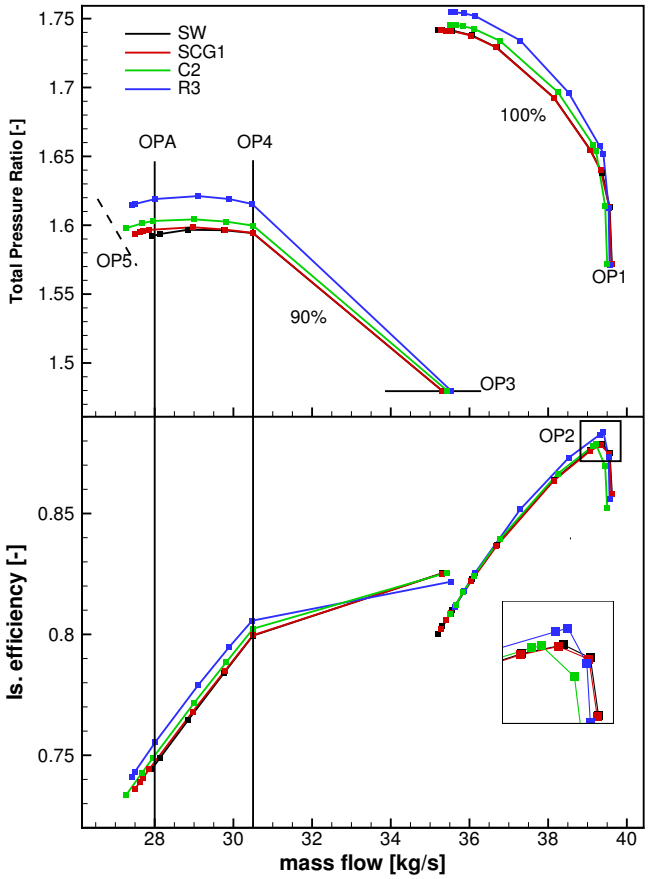

FIGURE 13. **Component (IGV-R1-S1) characteristics**

have an increased chord length at tip. It can be observed that along the Pareto front the chord lengths of profiles at mid height increase. This suggests that for the optimized rotor geometries not only the tip region is important for the surge margin but also the region around mid height. In general, when a blade is optimized regarding surge margin and efficiency it can be expected that the stability margin of the different blade sections along the height will become more uniform.

FURTHER ANALYSIS

For a comparison one Pareto optimal geometry of each optimization is chosen, SCG1, C2 and R3 (squares in fig. 6), and analyzed in relation to the smooth wall configuration.

Comparing the characteristics (fig. 13) of the grooved rotor and the reference smooth wall geometry, an increase in difference towards the stability limit can be observed, which can be explained by an increasing pressure difference between suction and pressure side towards the stability limit at the location of the groove. This is a typical feature of casing treatments. On the contrary the influence of the casing and rotor modification have a considerable influence on the whole map but also a higher surge margin increase.

From the three optimizations only the rotor optimization succeeded in reducing the rotor loss at design point (fig. 15) and at the same time increasing the surge margin. This has been achieved by a redistribution of the blade loading resulting in blades with reduced loading at tip and a weaker shock-vortex interaction. The same effect has been obtained by the casing optimization. The reduced tip-vortex shock interaction can be observed in figure 14 showing entropy contours at 98% height. A significantly reduced entropy rise can be observed for the optimized casing and rotor.

As the shock-vortex-interaction is the main mechanism the casing groove is influencing, a weaker effect of the cas-

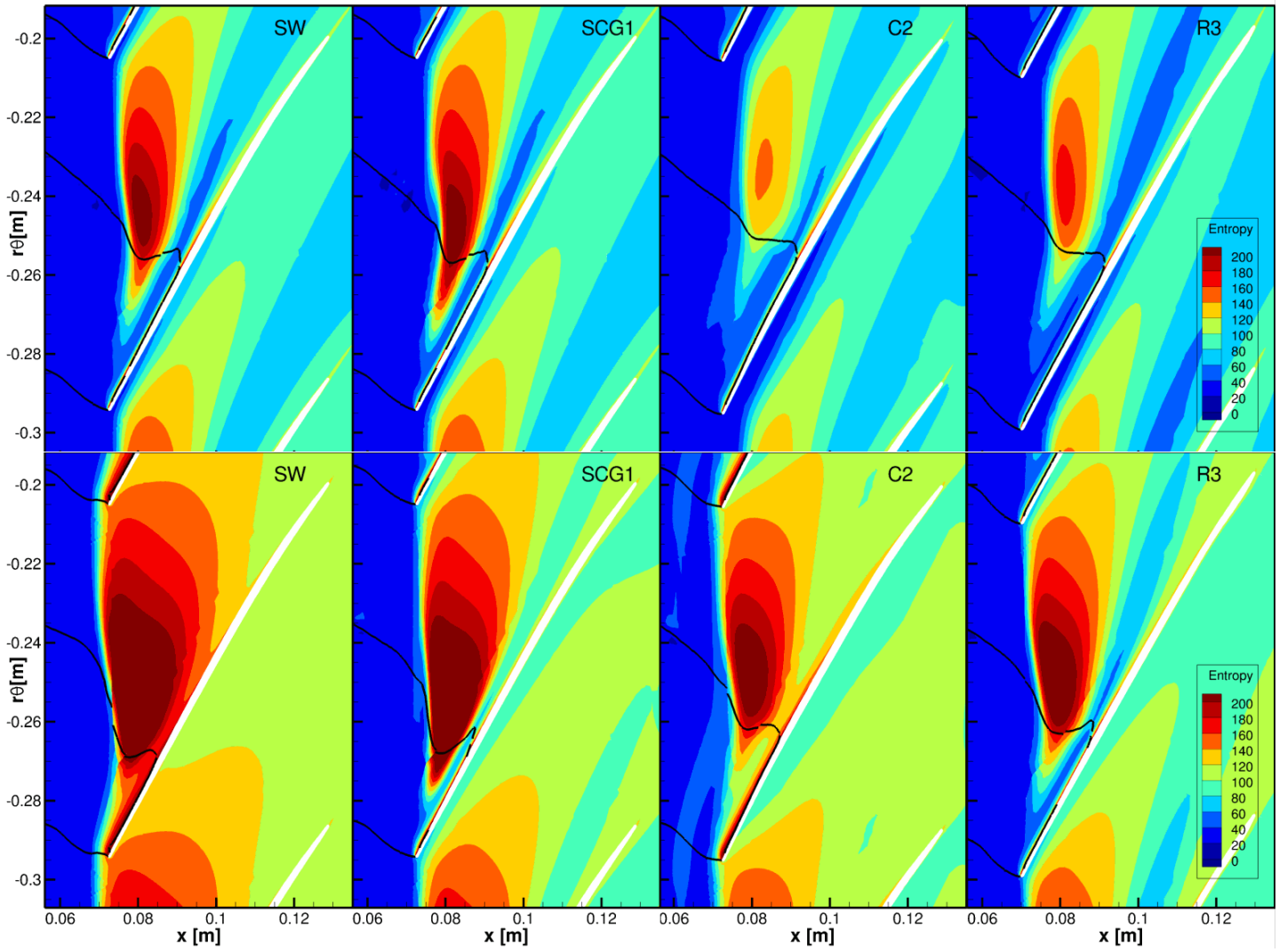

FIGURE 14. **Entropy plots at 98% channel height at OP4 (top) and near stall OPA (bottom)**

ing grooves has to be expected when used in conjunction with the optimized rotors. Three rotors (R1, R3, R4) have been simulated with the single groove SCG1. In all three cases a slight loss in peak efficiency has been observed, comparable to the loss obtained when simulating SCG1 with the reference rotor R0, but no significant gain in surge margin could be obtained (see fig. 6).

The same study has been conducted with selected optimized casing geometries, C2, C4 and C7 applying them to specific rotor geometries R1, R3 and R4. The resulting difference in the fitness function space can be observed in fig. 6. Examining the Pareto optimal rotor geometries R1 and R3 no big difference in surge margin has been obtained applying the modified casing geometries. This can be explained by the fact that both, optimized rotors and casings are reducing the loading at tip. As explained before, the stability margin of the different rotor sections, from hub to tip, for the Pareto optimal rotor geometries appear to be better matched. Therefore a further reduction of tip loading of the optimized rotor geometries through the casing contouring will result in an instability at a different height of the rotor. This hypothesis can be underlined by the following observation. Figure 15 shows the pressure loss at different operating points. At the stability limit (OP5) the optimized rotor R3 with smooth wall shows an equal maximum loss at 60% height as the same rotor in conjunction with casing C2 (the combination is denoted as R3C2). Comparing R3, C2 and the combination R3C2 at a similar mass flow near

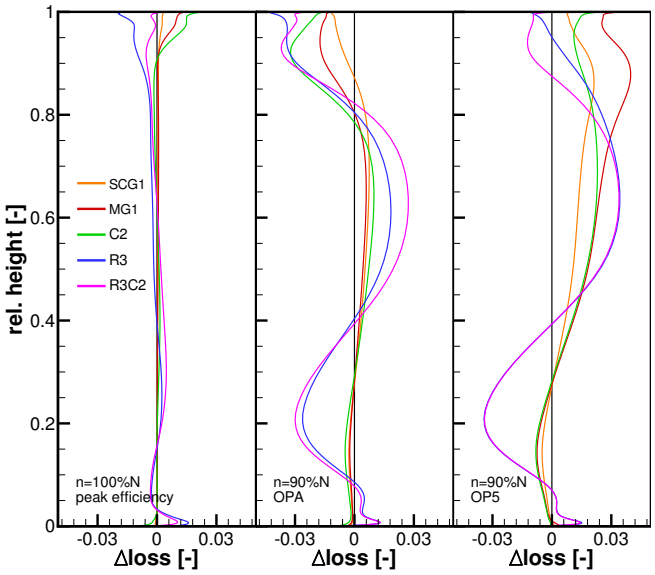

FIGURE 15. **Rotor pressure loss coefficient as a difference to the reference geometry at peak efficiency, OPA and OP5 for different geometries.**

surge (OPA) almost the same reduction in loss at tip can be observed for all cases indicating that the casing contouring C2 has no further effect close to the casing regarding a surge margin improvement when combined with R3. Considering a sub optimal (regarding the Pareto rank) rotor R4, a significantly higher influence of a casing contouring modification on the surge margin can be observed.

Examining the change in peak efficiency by the different casing geometries it can be observed that no Pareto optimal casing (C2, C4) could further improve the efficiency of R3. However casing C7 which has a significantly different shape in the front part (wave in the opposite direction) and is not redistributing the flow to the extend C2 and C4 do, as described before, has a slightly positive effect on rotor R3.

It can be concluded that a blind combination of separately optimized casing contouring, rotor geometry and casing treatment will not result in the desired effect, which is not very surprising. In this context it also has to be noticed that the combinations discussed above all fail to meet the constraints on mass flow and pressure ratio applied during the optimization. However if the effects are understood, a beneficial combination of rotor and casing modification together with a casing treatment seems feasible and will be subject of future optimization studies.

CONCLUSION

An optimization procedure for improving the surge margin and efficiency of transonic compressors has been presented. Three different optimizations have been performed. A circumferential groove, the casing above the rotor and the rotor have been optimized separately regarding surge margin and efficiency. Constraints were imposed in order to not to change the design point significantly. The structural mechanics were checked during the optimizations to avoid infeasible designs. Combinations of optimized geometries of all optimizations have been studied.

It has been found that a reduction of tip loading is the main effect that has led to an increase in surge margin reducing the shock and the shock-vortex interaction. The rotor geometries appear to have a better radial matching regarding the stability of the different blade sections from hub to tip. Therefore a simple combination with a casing contouring that is further reducing the loading at tip and radially redistributing the flow does not lead to an additional increase in surge margin.

A comparably small increase in surge margin has been obtained by optimizing a single circumferential groove. This gain could be increased by applying multiple grooves in the front region of the blade upwind of the position of the shock at the numerical stability limit. The grooves also affect the shock-vortex interaction, reducing the extent of the low momentum region which forms when the vortex bursts. All circumferential groove configurations showed a negative impact on the peak efficiency, increasing with the size and number of the grooves. Their positive effect on the surge margin diminishes when applied to optimized rotor configurations.

The effects that have been observed clearly show that a simple transferability of optimized casing treatments or casing contours on different rotors is not possible, especially if the rotor has been optimized for exactly the same objectives. It can be concluded that an overall optimum of the design can only be obtained if all parts of the design space are considered simultaneously. The knowledge of how geometrical changes of the casing, the rotor and in the form of casing treatments can affect the surge margin and efficiency can, however, be used in the early design phases of a compressor to improve the design.

REFERENCES

[1] Rabe, D. C., and Hah, C., 2002. "Application of Casing Circumferential Grooves for Improved Stall Margin in a Transonic Axial Compressor". *ASME Conference Proceedings,* ***2002***(3610X), pp. 1141–1153.

[2] Perrot, V., Touyeras, A., and Lucien, G., 2007. "Detailed CFD Analysis of a Grooved Casing Treatment on an Axial Subsonic Compressor". In 7th European Conference on Turbomachinery, pp. 305–316.

[3] Müller, M. W., Schiffer, H.-P., and Hah, C., 2007. "Effect of Circumferential Grooves on the Aerodynamic Performance of an Axial Single-Stage Transonic Compressor". *ASME Conference Proceedings,* ***2007***(47950), pp. 115–124.

[4] Houghton, T., and Day, I. J., 2011. "Enhancing the Stability of Subsonic Compressors Using Casing Grooves". *Journal of Turbomachinery,* ***133***(2), p. 021007.

[5] Houghton, T., and Day, I. J., 2012. "Stability Enhancement by Casing Grooves: The Importance of Stall Inception Mechanism and Solidity". *Journal of Turbomachinery,* ***134***(2), p. 021003.

[6] Wu, Y., Chu, W., Zhang, H., and Li, Q., 2010. "Parametric Investigation of Circumferential Grooves on Compressor Rotor Performance". *Journal of Fluids Engineering,* ***132***(12), p. 121103.

[7] Choi, K.-J., Kim, J.-h., and Kim, K.-Y., 2010. "Design Optimization of Circumferential Casing Grooves for a Transonic Axial Compressor to Enhance Stall Margin". In ASME Turbo Expo 2010: Power for Land, Sea and Air GT2010, pp. 1–9.

[8] Carnie, G., Wang, Y., Qin, N., and Shahpar, S., 2011. "Design Optimisation of Casing Grooves using the Zipper Layer Meshing Method". In Proceedings of ASME Turbo Expo, no. GT2011-45483.

[9] Johann, E., Nipkau, J., and Muck, B., 2008. "Experimental and Numerical Flutter Investigation of the 1St Stage Rotor in 4-Stage High Speed Compressor". In ASME Turbo Expo 2008: Power for Land, Sea and Air GT2008.

[10] Greitzer, E. M., Nikkanen, J. P., Haddad, D. E., Mazzawy, R. S., and Joslyn, H. D., 1979. "A Fundamental Criterion for the Application of Rotor Casing Treatment". *Journal of Fluids Engineering,* ***101***(2), p. 237.

[11] Ashcroft, G., Heitkamp, K., and Kuegeler, E., 2010. "High-order accurate implicit runge-kutta schemes for the simulation of unsteady flow phenomena in turbomachinery.". In 5th European Conference on Computational Fuild Dynamics ECCOMAS CFD.

[12] Becker, K., Heitkamp, K., and Kuegeler, E., 2010. "Recent progress in a hybrid-grid CFD solver for turbomachinery flows". In 5th European Conference on Computa- tional Fuild Dynamics ECCOMAS CFD.

[13] Voges, M., Schnell, R., Willert, C., Mönig, R., Müller, M. W., Zscherp, C., and Hoehe, L., 2011. "Investigation of Blade Tip Interaction With Casing Treatment in a Transonic Compressor, Part I: Particle Image Velocimetry". *Journal of Turbomachinery,* ***133***(1), p. 11007.

[14] Schönweitz, D., Voges, M., Goinis, G., Enders, G., and Johann, E., 2013. "Experimental and Numerical Examinations of a Transonic Compressor-Stage with Casing Treatment". In Proceedings of ASME Turbo Expo 2013: Turbine Technical Conference and Exposition GT2013, pp. 1–14.

[15] Reid, L., and Moore, R. D., 1978. Performance of Single-Stage Axial-Flow Transonic Compressor With Rotor and Stator Aspect Ratios of 1.19 and 1.26, Respectively, and With Design Pressure Ratio of 1.82. Tech. Rep. TP-1338, NASA, Lewis Research Center, Cleveland, Ohio.

[16] Aulich, M., and Siller, U., 2011. "High Dimensional Constrained Multiobjective Optimization of a Fan Stage". In ASME Turbo Expo, no. GT2011-45618.

[17] Voß, C., Aulich, M., and Raitor, T., 2014. "Metamodel assisted aeromechanical optimization of a transonic centrifugal compressor". In 15th International Symposium on Transport Phenomena and Dynamics of Rotating Machinery, ISROMAC-15.

[18] Kröger, G., Voß, C., Nicke, E., and Cornelius, C., 2011. "Theory and Application of Axisymmetric Endwall Contouring for Compressors". In ASME Turbo Expo 2011: Power for Land, Sea and Air GT2011.